Rapid Communications

Transformation of shock-compressed copper to the body-centered-cubic structure at 180 GPa

Surinder M. Sharma [1], Stefan J. Turneaure [1], J. M. Winey [1], and Y. M. Gupta [1,2,*]

[1] *Institute for Shock Physics, Washington State University, Pullman, Washington 99164, USA*

[2] *Department of Physics and Astronomy, Washington State University, Pullman, Washington 99164, USA*

(Received 10 June 2020; accepted 16 July 2020; published 29 July 2020)

Using *in situ* x-ray diffraction measurements in shock-compressed copper (38–276 GPa), we show that the ambient face-centered-cubic (fcc) structure transforms to the body-centered-cubic (bcc) structure at ∼180 GPa. Additionally, stacking fault (SF) abundance in shock-compressed copper increases with compression, reaching ∼10% at the onset of the fcc-bcc phase transition. Both findings are consistent with recent results on shock-compressed gold and silver that showed the importance of SFs in facilitating the fcc-bcc transformation. In contrast to our results, copper was recently reported to retain the fcc structure to over 1000 GPa under ramp compression [Fratanduono *et al.*, Phys. Rev. Lett. **124**, 015701 (2020)]. Further studies are needed to understand why the fcc-bcc transformation in copper is observed under shock compression, but not under ramp compression.

DOI: 10.1103/PhysRevB.102.020103

Shock-wave and static compression experiments, despite significantly different timescales, are widely used to examine compression-induced structural transformations in condensed matter. Because direct determination of crystal structures—using x-ray diffraction (XRD)—during shock compression has been experimentally difficult, identification of high-pressure phases in much of the shock-wave literature has relied on static pressure results. In utilizing static results to understand shock-compressed states, two common assumptions are the following: temperature is the primary difference between shock-wave response (adiabatic compression) and static pressure response (isothermal compression), particularly at high pressures (>50 GPa) [1,2]; and crystal structures during shock compression correspond to those achieved under comparable static compression [3]. Overall, *in situ* XRD measurements during shock compression have supported this correspondence in the limited number of materials examined [4–10].

We note that unlike the nearly isotropic compression achieved in static pressure experiments, a defining characteristic of shock-wave compression is uniaxial strain which leads to plastic deformation—resulting in microstructural changes, including lattice defects [11,12]. Effects of deformation-induced lattice defects on thermodynamic equations of state (EOS) and high-pressure phase changes have received minimal attention in shock-wave studies—including comparisons with static pressure results—because material phenomena due to density and deformation changes are generally considered to be uncoupled and because of the challenges associated with microstructural measurements during shock compression.

Due to recent experimental developments utilizing intense x-ray sources, real-time XRD measurements can now be obtained in shock-compression experiments to examine both pressure-induced phase changes [6–10,13–15] and deformation-induced microstructural changes [15–18]. Using synchrotron x rays, XRD measurements were utilized recently to examine the shock-compression response of three face-centered-cubic (fcc) metals: gold, silver, and platinum [13,15,18]. The novel findings from these studies, briefly summarized below, provided the motivation for the present work on copper.

The results on Au and Ag demonstrated that stacking faults (SFs) constitute an important deformation mechanism during shock compression. For both materials, the abundance of SFs increases with shock stress to ∼150 GPa where almost every sixth layer is a SF [15,18]. Beyond ∼150 GPa, both metals transform to the body-centered-cubic structure (bcc) [13,15]. Furthermore, Pt exhibited neither significant SF formation nor structural transformation when shock compressed to stresses reaching 380 GPa [15]. Taken together, the results on Au, Ag, and Pt show that SF formation is essential for the fcc-bcc transition not observed in static pressure experiments. Stacking fault energy (SFE) provides a way to understand these results as it is significantly higher for Pt, compared to Au and Ag [19–21]. Smaller SFE leads to shock-induced SF generation, which, in turn, facilitates the fcc-bcc phase transformation. Therefore, copper would be expected to behave similarly to Ag and Au since the SFE for Cu is somewhat higher than the Ag and Au SFEs, but much less than the Pt SFE (SFEs are 16, 32, 45, and 322 $\mathrm{mJ/m^2}$ for Ag, Au, Cu, and Pt, respectively) [19–21].

Copper is widely used both as an impactor and as an impedance-matching driver plate in shock experiments, and several studies have examined its Hugoniot curve [22–26]. These continuum results did not display any anomaly in the measured Hugoniot states up to 1.1 TPa [26]. However, sound velocity measurements under shock compression suggest probable melting at ∼230 GPa [27], in agreement with theoretical predictions [28]. Under static compression, the fcc structure of copper is known to be stable up to ∼150 GPa, the highest static pressure studied [29]. First-principles theoretical calculations predict the absence of any phase transformation in copper under static compression to 100 TPa

[*] ymgupta@wsu.edu

[30]. Therefore, similar to gold and silver, copper has been suggested and used as a pressure standard for high-pressure studies [29–32].

Copper has also been a subject of several studies investigating the deformation mechanisms of metals under shock compression. Although *postmortem* studies of shock-recovered copper samples have found a significant abundance of stacking faults [33–35], an *in situ* Laue x-ray-diffraction study reported results that did not exhibit features consistent with the generation of stacking faults in Cu shocked to ∼50 GPa [36]. In a recent investigation, copper was reported to retain its ambient fcc structure under ramp compression to 1.15 TPa [32]. Because the reported high-stress dynamic response of copper [32,36] differs significantly from that reported for gold and silver [13–15,18], determination of the structural and microstructural evolution in copper shock compressed to high stresses—up to the melt transition—is an important need.

Real time, x-ray-diffraction (XRD) measurements were obtained on copper shock compressed to ∼276 GPa at the laser-shock experimental station [37] of the Dynamic Compression Sector (DCS) located at the Advanced Photon Source. The experimental configuration, shown schematically in Fig. 1, is similar to the configuration used in recent laser-shock compression experiments on other noble metals [13,15,18]. In these experiments, a 100 J laser was used to ablate an aluminized Kapton film, launching a shock wave in the Kapton, which then propagated into a 20-μm-thick polycrystalline copper foil (Goodfellow, 99.99+% pure). The temper of the Cu foil was "as rolled" and the ambient XRD patterns displayed intensity variations around the diffraction rings indicating texture, typical of rolled metals (see Supplemental Material (SM) Fig. S1 [38] for representative ambient two-dimensional Cu diffraction images). Flat-top shock states in the copper foil samples, with stresses ranging from 38 to 276 GPa, were generated using one of the two different pulse durations (5 or 10 ns) along with beam splitters to control the total laser energy reaching the target [37].

Laser-shock experiments on copper were performed at nine different stresses. Shock stresses were determined from velocity interferometry measurements that recorded the velocity histories at the Cu/LiF window interface (see Fig. S2 [38]). For seven of the nine shock stresses, a companion experiment was performed without a LiF window. For these experiments, the same laser-drive settings were used as those for the corresponding experiments with a LiF window. These companion experiments had cleaner XRD records because of the absence of LiF Laue XRD spots, reduced x-ray absorption, and reduced incoherent scattering reaching the detector. The shock stresses for the companion experiments are assumed to be the same as those determined from the corresponding experiments with a LiF window, since the laser-drive histories for companion experiments with and without LiF windows were nominally the same. Shock stresses and results for 17 laser-shock experiments on copper are listed in Table S1 [38]. Lattice parameters for shocked Cu, determined from the *in situ* XRD measurements, are consistent between companion experiments with and without a LiF window (see Table S1 [38]). More details regarding laser-shock experiments at the DCS can be found in Ref. [37].

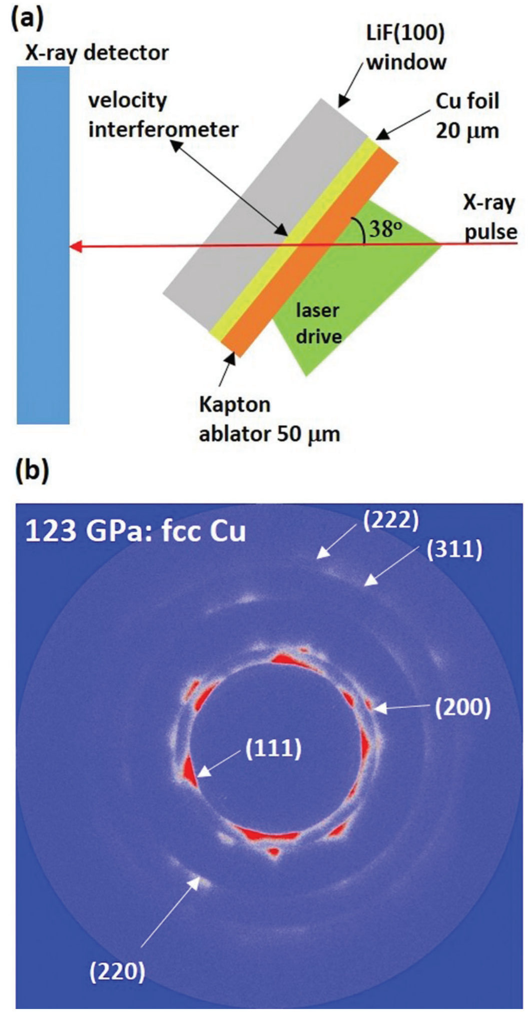

FIG. 1. (a) Experimental configuration used for *in situ* XRD measurements in copper laser shocked to stresses from 38 to 276 GPa. For some experiments, a LiF window was not used. (b) Representative XRD results for fcc copper at 123 GPa. Result is from experiment 8 which did not include a LiF window.

The compression and crystal structure of the shocked copper samples were probed using XRD measurements while the high-stress (38–276 GPa) shock wave propagated through the Cu sample. The XRD measurements correspond to a snapshot obtained using an ∼100-ps-duration x-ray pulse with maximum flux at ∼23.5 keV and an energy bandwidth of a few percent (see Fig. S3). The XRD patterns were recorded before the shock wave reflects from the LiF window or from the Cu-free surface (resulting in a partial or full stress release, respectively) and before a release wave from the ablator enters the Cu sample. Thus, the XRD measurements have contributions from two distinct material states: the shocked state and the ambient state.

Powder XRD patterns were recorded on a Rayonix SX165 area detector, capturing the first five diffraction rings of the fcc copper. The two-dimensional diffraction patterns are reduced to one-dimensional line profiles of intensity versus scattering angle (2θ) by azimuthally integrating around the rings using FIT2D [40]. For targets that had a LiF window, the LiF Laue diffraction spots were masked prior to performing the azimuthal integration. Because the measured XRD profiles contained diffraction from both shocked and unshocked Cu, a fraction of the ambient XRD line profile (measured from the Cu sample prior to each shock compression experiment) was subtracted from the XRD line profile measured during the shock experiment to obtain the XRD line profile corresponding to the shocked copper, as described in Ref. [18].

To identify structural changes (volume compression, stacking fault generation, and/or phase transformations) under shock compression, the experimental XRD line profiles are quantitatively compared with simulated line profiles. The simulated profiles are computed by incorporating all the relevant experimental parameters: sample thickness, angle of incidence Φ of the x-ray beam with respect to the sample plane, sample to detector distance, spectral flux of x rays incident on the sample, x-ray absorption and line broadening due to instrumental resolution. The effects of SFs on line profiles are incorporated in the simulations using the formalism developed by Warren [41] and generalized by Velterop *et al.* [42]. Finite SF probability results in a shift of the (200) diffraction peak toward the (111) diffraction peak [18,41,42]. Simulated diffraction profiles are also convoluted with a Lorentzian broadening function to match the observed peak widths; these peak widths increase with shock stress, as also observed previously for gold and silver [15,18]. When fitting simulations to the measured line profiles, the relative intensities of different simulated $\{hkl\}$ peaks are varied, which accounts for the textured nature of the copper foils. A more detailed description of the forward XRD simulations is given in Ref. [18].

Figure 2 shows measured XRD line profiles for Cu, along with the simulated XRD line profiles incorporating SFs in the fcc structure at several representative stresses. The corresponding two-dimensional XRD patterns recorded in the ambient state and in the shock experiments are shown in Fig. S1 of the Supplemental Material [38]. Up to ∼157 GPa, the line profiles show that the Cu remains in the fcc phase. However, XRD simulations only match the measured fcc peak positions when SFs are included (see Fig. S4). The SF probability increases with compression reaching ∼10% at ∼180 GPa, as shown in Fig. 3. The observed variation in the SF probability with volume compression is qualitatively similar to molecular-dynamics simulation results [33,34,44], as well as to the experimental results for silver [15] and gold [18] (see Fig. S5). However, the SF probability is lower for Cu than for Au and Ag at a given volume compression.

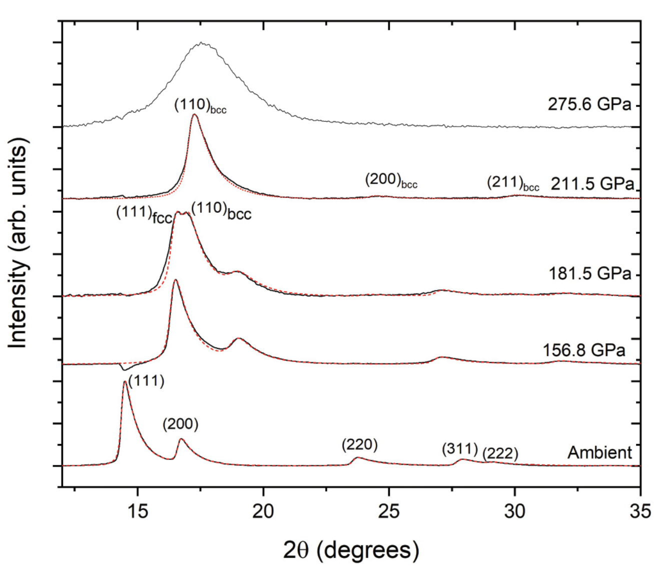

FIG. 2. Representative x-ray-diffraction line profiles at various stresses, indicating the fcc phase at stresses below 181.5 GPa, mixed fcc-bcc phases at 181.5 GPa, and bcc phases at higher stresses up to the shock melting stress. At 275.6 GPa, the diffraction profile has only one broad diffraction peak at ∼17.5° scattering angle, indicating complete melting of the shocked copper. The experiments corresponding to these line profiles are indicated in Table S1 [38].

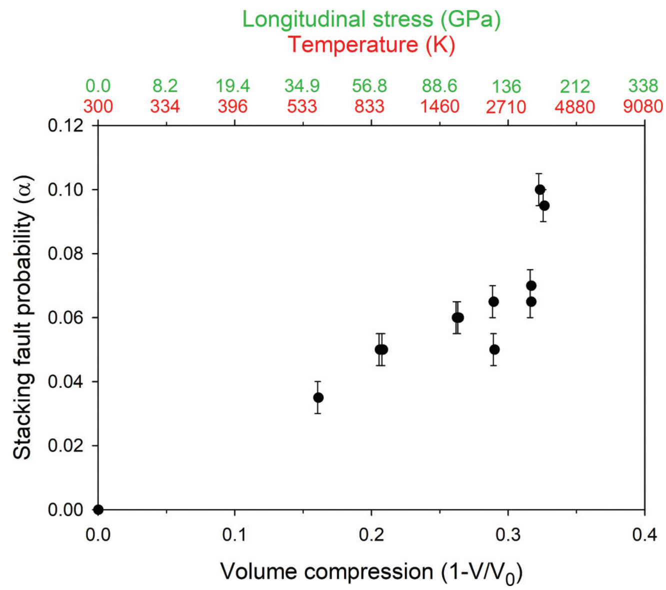

FIG. 3. Stacking fault probability (α) in copper versus volume compression. The corresponding Hugoniot stresses and calculated temperatures are shown at the top. The longitudinal stresses were determined using the reported Cu Hugoniot [22–24,45]. The calculated temperatures were determined using an equation of state (#3336) from the SESAME library developed at Los Alamos National Laboratory [43].

The line profile for Cu at ∼182 GPa shows the appearance of a new peak indexed as the {110} bcc peak that partially overlaps with the {111} fcc peak (Fig. 2), indicating a mixed fcc-bcc phase. At ∼212 GPa, the fcc peaks completely vanish and two additional new diffraction peaks are apparent at $2\theta \approx 24.5^\circ$ and 30° (Fig. 2). These two new peaks are indexed as {200} and {211} bcc peaks, respectively. From the width of the {110} bcc peak, the coherently diffracting domain size is estimated to be ∼22 nm at ∼212 GPa. At ∼276 GPa, the crystalline diffraction peaks are replaced by a significantly broader diffraction peak at $2\theta \approx 17.5^\circ$, indicating the molten phase.

Figure 4 shows that the peak longitudinal stress (P_x)–volume (V) states determined from the present experiments are in good agreement with the previously reported Hugoniot curve from continuum measurements [22–24,45]. The lack of a discontinuity in the previous Hugoniot data indicates a small volume change for the fcc-bcc transition. Our XRD results confirm this finding as the volume/atom in the mixed-phase

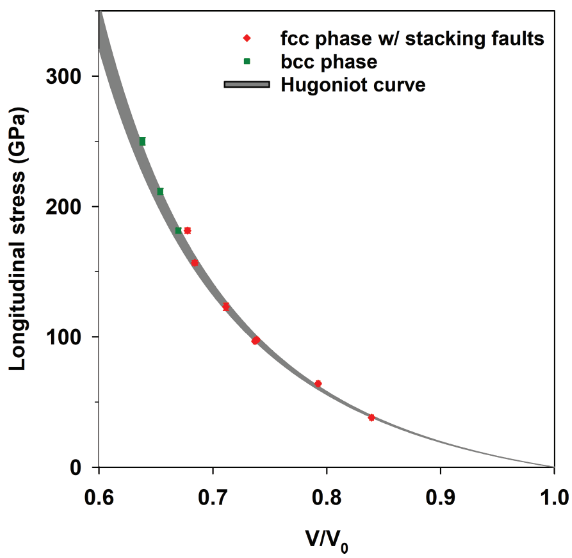

FIG. 4. Measured P_x-V states for shock-compressed copper. The stresses were determined from the velocity interferometry results and the volumes were determined from the XRD results. For comparison, the gray band is the Hugoniot curve for Cu [45], determined from continuum measurements [22–24]; the width of the band indicates the experimental uncertainty.

region differs by ∼1% for the fcc and bcc structures, which is on the order of the experimental resolution.

The present experimental results establish two important findings: (1) Shock compression of copper generates an increasing abundance of stacking faults with increasing compression and (2) shock-compressed copper adopts the bcc structure above 180 GPa. Both of these phenomena were also observed in shock-compressed gold [13,18] and silver [15]. In particular, our observation of a shock-induced first-order fcc-bcc transformation in copper—similar to that observed in shock-compressed gold [13] and silver [15], but not in platinum [15]—supports our earlier conclusion that SFs provide sites essential for the bcc phase and, hence, represent a necessary condition for this transformation.

The above findings are in marked contrast to previous results for dynamically compressed copper [32,36]. Our observation of stacking faults under shock compression differs from earlier *in situ* XRD results on laser-shocked Cu that found no evidence for SFs in copper shock compressed to ∼50 GPa [36]. However, it is important to recognize that the SF probability at 50 GPa is low (∼4% based on the present work) and, therefore, the expected changes in the {200} Cu peaks may have been too small to be observed in the broad Laue diffraction images reported in the previous experiments [36]. Similarly, the presence of stacking faults and/or other potential defects was not noted in Ref. [32] for Cu ramp compressed up to 1.15 TPa. However, the diffraction pattern reported in Ref. [32] has broad peaks, some of which are obscured by diffraction from ambient platinum (used for angle calibration), likely making it impossible to draw conclusions regarding the presence of stacking faults.

The present finding regarding the fcc-bcc transition differs markedly from the recent *in situ* XRD results for ramp-compressed Cu where the fcc phase is claimed to persist to 1.15 TPa [32]. Although ramp compression and shock compression both generate a uniaxially strained state, the loading rates are significantly different. Assuming that the conclusions of Ref. [32] are correct, then these contrasting findings suggest the possibility of a critical loading rate above which the material response undergoes a dramatic change.

Ramp compression of Cu to a given peak stress will have a lower temperature than Cu shock compressed to the same peak stress. Although this temperature difference could be invoked as a possible explanation for the apparent lack of the fcc-bcc transformation in ramp compressed Cu, our recent *in situ* XRD results showed a lack of stacking faults and the persistence of the fcc phase in shock compressed Pt to ∼380 GPa [15]. In addition, the pressures and temperatures associated with onset of the fcc-bcc transformation in shock-compressed Cu, Ag, and Au are not close to any known equilibrium-phase boundaries, including the melt boundary [13,15]. Hence, temperature alone is likely not the governing factor driving the fcc-bcc transformation in dynamically compressed noble metals.

Since stacking faults have an element-specific formation energy, which is predicted to increase rapidly with compression [46,47], activation of stacking faults may be hindered at the lower temperatures encountered in ramp compressed Cu. As discussed above, the occurrence of the fcc-bcc phase transformation and the presence of shock-induced SFs below the transformation onset show a clear link for noble metals. Therefore, the absence of SFs in ramp-compressed Cu would be consistent with an absence of the fcc-bcc phase transformation, the same as observed for shock-compressed Pt [15]. An unambiguous resolution of these issues requires *in situ* XRD measurements on ramp-compressed fcc metals with sufficient resolution to quantify stacking-fault probabilities. Such studies would elucidate possible fundamental differences in the microscopic nature of the peak states achieved under shock compression and ramp compression. Additionally, the contrasting experimental findings between shock compressed and ramp-compressed Cu should motivate further theoretical work to examine the effect of loading rate on deformation and structural transformations in dynamically compressed noble metals.

Finally, earlier theoretical investigations [48] have predicted the possibility of virtual melting and rapid resolidification in copper under laser shock compression at stresses of ∼160 GPa, i.e., at stresses lower than in the present experiments. Our results do not support the existence of such a phenomenon.

Paulo Rigg, Pinaki Das, Kory Green, Ray Gunawidjaja, Yuelin Li, Korey Mercer, Drew Rickerson, Adam Schuman, Nick Sinclair, Xiaoming Wang, Brendan Williams, Jun Zhang, and Robert Zill at the Dynamic Compression Sector (Advanced Photon Source, Argonne National Laboratory) are gratefully acknowledged for their expert assistance with the experiments. Yoshi Toyoda is thanked for assistance with the experiments and with analysis of velocity interferometry data. The work reported here was supported by the U.S. Department of Energy (DOE), National Nuclear Security Administration (NNSA) under Awards No. DE-NA0002007 and No. DE-NA0003957. This publication is also based upon work performed at the Dynamic Compression Sector, operated by Washington State University under DOE/NNSA Award No. DE-NA0002442. This research used resources of the Advanced Photon Source, a DOE Office of Science User Facility operated for the DOE Office of Science by Argonne National Laboratory under Contract No. DE-AC02-06CH11357.

[1] W. J. Nellis, J. A. Moriarty, A. C. Mitchell, M. Ross, R. G. Dandrea, N. W. Ashcroft, N. C. Holmes, and G. R. Gathers, Phys Rev. Lett. **60**, 1414 (1988).

[2] H. K. Mao and P. M. Bell, J. W. Shaner, and D. J. Steinberg, J. Appl. Phys. **49**, 3276 (1978).

[3] G. E. Duvall and R. A. Graham, Rev. Mod. Phys. **49**, 523 (1977).

[4] T. d'Almeida and Y. M. Gupta, Phys. Rev. Lett. **85**, 330 (2000).

[5] D. H. Kalantar, J. F. Belak, G. W. Collins, J. D. Colvin, H. M. Davies, J. H. Eggert, T. C. Germann, J. Hawreliak, B. L. Holian, K. Kadau *et al.*, Phys. Rev. Lett. **95**, 075502 (2005).

[6] S. J. Turneaure, N. Sinclair, and Y. M. Gupta, Phys. Rev. Lett. **117**, 045502 (2016).

[7] P. Kalita, P. Specht, S. Root, N. Sinclair, A. Schuman, M. White, A. L. Cornelius, J. Smith, and S. Sinogeikin, Phys. Rev. Lett. **119**, 255701 (2017).

[8] S. J. Tracy, S. J. Turneaure, and T. S. Duffy, Phys. Rev. Lett. **120**, 135702 (2018).

[9] E. E. McBride, A. Krygier, A. Ehnes, E. Galtier, M. Harmand, Z. Konôpková, H. J. Lee, H.-P. Liermann, B. Nagler, A. Pelka *et al.*, Nat. Phys. **15**, 89 (2019).

[10] P. Renganathan, S. J. Turneaure, S. M. Sharma, and Y. M. Gupta, Phys. Rev. B **99**, 134101 (2019).

[11] C. S. Smith, Trans. TMS-AIME **212**, 574 (1958).

[12] M. A. Meyers, Scr. Metall. **12**, 21 (1978).

[13] S. M. Sharma, S. J. Turneaure, J. M. Winey, Y. Li, P. A. Rigg, A. Schuman, N. Sinclair, Y. Toyoda, X. Wang, N. Weir, J. Zhang, and Y. M. Gupta, Phys. Rev. Lett. **123**, 045702 (2019).

[14] R. Briggs, F. Coppari, M. G. Gorman, R. F. Smith, S. J. Tracy, A. L. Coleman, A. Fernandez-Pañella, M. Millot, J. H. Eggert, and D. E. Fratanduono, Phys. Rev. Lett. **123**, 045701 (2019).

[15] S. M. Sharma, S. J. Turneaure, J. M. Winey, and Y. M. Gupta, Phys. Rev. Lett. **124**, 235701 (2020).

[16] C. E. Wehrenberg, D. McGonegle, C. Bolme, A. Higginbotham, A. Lazicki, H. J. Lee, B. Nagler, H.-S. Park, B. A. Remington, R. E. Rudd, M. Sliwa, M. Suggit, D. Swift, F. Tavella, L. Zepeda-Ruiz, and J. S. Wark, Nature (London) **550**, 496 (2017).

[17] S. J. Turneaure, P. Renganathan, J. M. Winey, and Y. M. Gupta, Phys. Rev. Lett. **120**, 265503 (2018).

[18] S. M. Sharma, S. J. Turneaure, J. M. Winey, P. A. Rigg, N. Sinclair, X. Wang, Y. Toyoda, and Y. M. Gupta, Phys. Rev. X **10**, 011010 (2020).

[19] J. P. Hirth and J. Lothe, *Theory of Dislocations*, 2nd ed. (McGraw-Hill, New York, 1982).

[20] P. C. J. Gallagher, Metall. Trans. **1**, 2429 (1970).

[21] R. Li, S. Lu, D. Kim, S. Schönecker, J. Zhao, S. K. Kwon, and L. Vitos, J. Phys.: Condens. Matter **28**, 395001 (2016).

[22] *LASL Shock Hugoniot Data*, edited by S. P. Marsh (University of California Press, Los Angeles, 1980), p. 57.

[23] L. V. Altshuler, A. A. Bakanova, I. P. Dudoladov, E. A. Dynin, R. F. Trunin, and B. S. Chekin, J. Appl. Mech. Tech. Phys. **22**, 145 (1981).

[24] A. C. Mitchell and W. J. Nellis, J. Appl. Phys. **52**, 3363 (1981).

[25] A. C. Mitchell, W. J. Nellis, J. A. Moriarty, R. A. Heinle, N. C. Holmes, R. E. Tipton, and G. W. Repp, J. Appl. Phys. **69**, 2981 (1991).

[26] C. A. McCoy, M. D. Knudson, and S. Root, Phys. Rev. B **96**, 174109 (2017).

[27] D. Hayes, R. S. Hixson, and R. G. McQueen, in *Shock Compression of Condensed Matter - 1999*, edited by M. D. Furnish, L. C. Chhabildas, and R. S. Hixson (American Institute of Physics, New York, 2000), p. 483.

[28] J. A. Moriarty, in *Shock Waves in Condensed Matter*, edited by Y. M. Gupta (Plenum, New York, 1986), p.101.

[29] A. Dewaele, P. Loubeyre, and M. Mezouar, Phys. Rev. B **70**, 094112 (2004).

[30] C. W. Greeff, J. C. Boettger, M. J. Graf, and J. D. Johnson, J. Phys. Chem. Solids **67**, 2033 (2006).

[31] R. G. Kraus, J.-P. Davis, C. T. Seagle, D. E. Fratanduono, D. C. Swift, J. L. Brown, and J. H. Eggert, Phys. Rev. B **93**, 134105 (2016).

[32] D. E. Fratanduono, R. F. Smith, S. J. Ali, D. G. Braun, A. Fernandez-Pañella, S. Zhang, R. G. Kraus, F. Coppari, J. M. McNaney, M. C. Marshall, L. E. Kirch, D. C. Swift, M. Millot, J. K. Wicks, and J. H. Eggert, Phys. Rev. Lett. **124**, 015701 (2020).

[33] B. Cao, E. M. Bringa, and M. A. Meyers, Metall. Mater. Trans. A **38**, 2681 (2007).

[34] H. N. Jarmakani, E. M. Bringa, P. Erhart, B. A. Remington, Y. M. Wang, N. Q. Vo, and M. A. Meyers, Acta Mater. **56**, 5584 (2008).

[35] M. A. Meyers, M. S. Schneider, H. Jarmakani, B. Kad, B. A. Remington, D. H. Kalantar, J. McNaney, B. Cao, and J. Wark, Metall. Mater. Trans. A **39**, 304 (2008).

[36] M. J. Suggit, A. Higginbotham, J. A. Hawreliak, G. Mogni, G. Kimminau, P. Dunne, A. J. Comley, N. Park, B. A. Remington, and J. S. Wark, Nat. Commun. **3**, 1224 (2012).

[37] X. Wang, P. Rigg, J. Sethian, N. Sinclair, N. Weir, B. Williams, J. Zhang, J. Hawreliak, Y. Toyoda, Y. M. Gupta, Y. Li, D. Broege, J. Bromage, R. Earley, D. Guy, and J. Zuegel, Rev. Sci. Instrum. **90**, 053901 (2019).

[38] See Supplemental Material at http://link.aps.org/supplemental/10.1103/PhysRevB.102.020103 for a table of experimental results and additional supporting figures. Supplemental Material includes Ref. [39].

[39] L. M. Barker and R. E. Hollenbach, J. Appl. Phys. **43**, 4669 (1972).

[40] A. P. Hammersley, ESRF Internal Report No. ESRF97 - HA02T (1997).

[41] B. E. Warren, *X-Ray Diffraction* (Addison-Wesley, Reading, 1969).

[42] L. Velterop, R. Delhez, T. H. De Keijser, E. J. Mittemeijer, and D. Reefman, J. Appl. Crystallogr. **33**, 296 (2000).

[43] SESAME: The Los Alamos National Laboratory Equation of State Database, edited by S. P. Lyon and J. D. Johnson,

Los Alamos National Laboratory Tech. Rep. LA-UR-92-3407 (1992).

[44] B. L. Holian and P. S. Lomdahl, Science **280**, 2085 (1998).

[45] P. A. Rigg, M. D. Knudson, R. J. Scharff, and R. S. Hixson, J. Appl. Phys. **116**, 033515 (2014).

[46] P. S. Branicio, J. Y. Zhang, and D. J. Srolovitz, Phys. Rev. B **88**, 064104 (2013).

[47] P. Andric, B. Yin, and W. A. Curtin, J. Mech. Phys. Solids **122**, 262 (2019).

[48] V. I. Levitas and R. Ravelo, Proc. Natl. Acad. Sci. USA **109**, 13204 (2012).